Chemical turbulence and standing waves in a surface reaction model: The influence of global coupling and wave instabilities

Cite as: Chaos 4, 499 (1994); https://doi.org/10.1063/1.166028
Submitted: 10 May 1994 • Accepted: 17 July 1994 • Published Online: 04 June 1998

M. Bär, M. Hildebrand, M. Eiswirth, et al.

Chemical turbulence and standing waves in a surface reaction model: The influence of global coupling and wave instabilities

M. Bär, M. Hildebrand, and M. Eiswirth
Fritz-Haber-Institut der Max-Planck-Gesellschaft, Faradayweg 4-6, D-14195 Berlin, Germany

M. Falcke and H. Engel
AG "Dissipative Strukturen," Institut für Theoretische Physik der TU Berlin, Rudower Chaussee 5, D-12489 Berlin, Germany

M. Neufeld
Institut für Theoretische Physik der Universität Stuttgart, Pfaffenwaldring 57, D-70550 Stuttgart, Germany

(Received 10 May 1994; accepted for publication 17 July 1994)

Among heterogeneously catalyzed chemical reactions, the CO oxidation on the Pt(110) surface under vacuum conditions offers probably the greatest wealth of spontaneous formation of spatial patterns. Spirals, fronts, and solitary pulses were detected at low surface temperatures ($T<500$ K), in line with the standard phenomenology of bistable, excitable, and oscillatory reaction-diffusion systems. At high temperatures ($T>540$ K), more surprising features like chemical turbulence and standing waves appeared in the experiments. Herein, we study a realistic reaction-diffusion model of this system, with respect to the latter phenomena. In particular, we deal both with the influence of global coupling through the gas phase on the oscillatory reaction and the possibility of wave instabilities under excitable conditions. Gas-phase coupling is shown to either synchronize the oscillations or to yield turbulence and standing structures. The latter findings are closely related to clustering in networks of coupled oscillators and indicate a dominance of the global gas-phase coupling over local coupling via surface diffusion. In the excitable regime wave instabilities in one and two dimensions have been discovered. In one dimension, pulses become unstable due to a vanishing of the refractory zone. In two dimensions, turbulence can also emerge due to spiral breakup, which results from a violation of the dispersion relation.

I. INTRODUCTION

Recent years have seen a rapid development of experimental and theoretical investigations in the field of pattern formation under nonequilibrium conditions.[1] On the experimental side, prototype systems like the Rayleigh–Bénard convection in physics[2] and the Belousov–Zhabotinsky (BZ) reaction in chemistry[3,4] have been exploited exhaustively. Theory has focused on investigations of general properties in the vicinity of the onset of instability,[1,5] as well as on considerations of reaction-diffusion models like the Oregonator for the BZ reaction.[6,7]

Here, we present a model for the CO oxidation on the Pt(110) surface under vacuum conditions,[8] which is based on the elementary steps of the reaction[9] and includes spatial coupling via surface diffusion of CO and the interplay between the reaction and the gas phase.[10] This reaction exhibits a great variety of spatial patterns,[11,12] and is particularly attractive to the model for several reasons: The system is strictly two dimensional and isothermal, because it only takes place in the surface adlayer and the heat of reaction is quickly absorbed by the platinum crystal. Moreover, there are only two reactant species, adsorbed CO and O, which form CO_2 in a single reaction step. The external control parameters are given by the partial pressures of CO and O_2 and the surface temperature T. They can be adjusted independently.

Beyond these favorable aspects, a handful of new features come into play. As in several heterogeneous systems, the interaction between the adsorbate layer and the surface structure has to be taken into account. The system possesses a global coupling through the gas phase, which can provide a rapid synchronization of the whole surface, and competes with a local coupling by surface diffusion of CO in the μm range. Further details of the model will be explained in the next section. The outline of the paper is as follows: First, we will consider the spatiotemporal dynamics under locally oscillatory conditions. In this case, any local change in the reaction rate affects the partial pressures of CO and O_2, whereby a global feedback on the whole surface is mediated. If the feedback strength exceeds a critical value, nontrivial effects like turbulence and standing waves occur in an otherwise homogeneously oscillating system.

In the second part, waves under excitable conditions will be considered. In contrast to other excitable media, the CO-oxidation model reveals wave instabilities upon change of the parameters. In one spatial dimension, pulses can lose the property of refractoriness. Thus, new pulses can be excited in the wake of the original pulse ("backfiring"). Spiral breakup in two dimensions emerges, if the selected spiral frequency violates the dispersion relation of the medium. Then a state with a fluctuating number of topological defects (i.e., spiral tips) is reached, phenomenologically similar to defect-mediated or amplitude turbulence in the complex Ginzburg–Landau equation.[13,14]

II. THE MODEL

The CO oxidation on Pt(110) proceeds via the classical Langmuir–Hinshelwood mechanism,[15] whereby the CO-driven structural change of the Pt(110) surface needs to be taken into account:

 1054-1500/94/4(3)/499/10/$6.00

$$CO_g + * \leftrightarrow CO_{ad},$$

$$O_{2,g} + 2* \rightarrow 2\ O_{ad},$$

$$O_{ad} + CO_{ad} \xrightarrow{CO_{ad}} 2* + CO_{2,g},$$

$$1\times 2 \leftrightarrow 1\times 1.$$

(Here $*$ denotes an empty adsorption site, suffices g, and ad distinguish gaseous and adsorbed species.) The CO absorption follows a precursor kinetics.[16] Moreover, the model should include the asymmetric inhibition, i.e., oxygen adsorption is forbidden on CO-covered sites, but not vice versa.

The sticking coefficient of oxygen depends on the surface structure. Thus three variables—the CO and O coverages u and v, and the 1×1 coverage w—remain, leading to the kinetic equations, which describe the reconstruction model of the CO oxidation on Pt(110):[9]

$$\frac{\partial u}{\partial t} = k_u s_u p_{CO}\left[1-\left(\frac{u}{u_s}\right)^3\right] - k_2 u - k_3 uv + \mathbf{D}\,\Delta u \tag{1a}$$

$$\frac{\partial v}{\partial t} = k_v p_{O_2}[s_{v1} w + s_{v2}(1-w)]\left[1-\left(\frac{u}{u_s}\right)-\left(\frac{v}{v_s}\right)\right]^2 - k_3 uv, \tag{1b}$$

$$\frac{\partial w}{\partial t} = k_5[f(u)-w]. \tag{1c}$$

The external control parameters here are the partial pressures of CO and oxygen, p_{CO} and p_{O_2}, and the crystal temperature T, which enters into the rates k_2, k_3, and k_5 through an Arrhenius dependence. Here, $f(u)$ has a sigmoid shape, as determined experimentally in LEED and STM studies. The constants are summarized in Table I: see Ref. 9 for details and experimental determination.

Spatial coupling is introduced through CO diffusion, compared to which O diffusion is very small.[17,18] Diffusion on the Pt(110) surface is anisotropic, i.e., $\mathbf{D}$ consists of the diffusion constants in the $[1\bar{1}0]$ and [001] crystallographic orientations:

$$\mathbf{D}\,\Delta u = D_x \frac{\partial^2 u}{\partial x^2} + D_y \frac{\partial^2 u}{\partial y^2}. \tag{1d}$$

From now on, the anisotropy of diffusion is neglected by scaling both diffusion constants D_x and D_y to unity by appropriate length transformations. The absolute length scales in Sec. III result from a diffusion constant of 10^{-10} m^2 s^{-1}. For a detailed discussion of Eqs. (1a)–(1d), the reader is referred to earlier work.[9,19]

A bifurcation analysis of the reaction part of Eq. (1) revealed regions with bistable, oscillatory, and excitable kinetics.[9] The complete reaction-diffusion equations were utilized to study the dynamics of fronts, pulses and spiral waves[20,22] in the model. Surface defects of mesoscopic size (μm) were shown to play an important role in the formation of waves. They are responsible for the unusual behavior of solitary pulses, including soliton-like collisions and wave splitting,[19] as well as for the coexistence of spiral waves with largely different wavelengths.[22,23] Nevertheless, the model calculations in this paper were all done with a spatially homogeneous medium.

The full system (1) was integrated using a semi-implicit procedure with periodic boundary conditions $\Delta x = 0.2$ and Δt below $\frac{1}{3}$ of the stability boundary. For the simplified model in the excitable regime, an explicit first-order Euler procedure was sufficient.

III. GLOBAL COUPLING IN THE OSCILLATORY REGIME

In addition to the surface diffusion introduced in Eqs. (1), there exist another spatial interaction between different parts of the Pt surface—the gas-phase coupling. During the oscillatory reaction the partial pressure of CO sways periodically.[10] This can be traced back to the temporal variations of the overall adsorption and desorption rates. Consequently, the CO partial pressure p_{CO} should be treated as a fourth variable. This is achieved by supplementing Eqs. (1) with the balance equation for CO:[24]

$$\frac{dp_{CO}}{dt} = \frac{J_{io}}{V}\left[p_{COe} - p_{CO}\left(1 + \frac{V_{ML}}{J_{io}A}\int_A dr^2\left\{k_1 p_{CO}\left[1-\left(\frac{u}{u_s}\right)^3\right] - k_2 u\right\}\right)\right]. \tag{2}$$

The constant J_{io} denotes the in- and outflux of gas in the reactor, V is the volume of the vacuum chamber, p_{COe} is the CO pressure in the gas inlet, and A is the area of the catalytic surface. These and other constants used in the simulations of Eqs. (1) and (2) are displayed in Table I. Since the mean-free path of the gas particles is much larger than the crystal size under-vacuum conditions, spatial variations of p_{CO} can be neglected. The integral term in Eq. (2) is taken over the whole surface. The strength of the global coupling depends on the parameter V_{ML}, which corresponds to the volume one monolayer of CO would have under the applied conditions (computed from the ideal gas law). For a crystal size of 1 cm^2 the value of V_{ML} is *ca.* 0.37, 1 ML^{-1} under typical experimental conditions ($p_{CO} = 10^{-4}$ Torr and $T = 500$ K). The corresponding variation of p_{O_2} is much smaller in relative amplitude, since under oscillatory conditions oxygen is always present in significant excess. Therefore, gas-phase coupling mediated by O_2 is neglected. A more detailed derivation of the gas-phase coupling and its implications was presented in Refs. 10 and 24.

Before presenting results on pattern formation, we take a short look at the bifurcation behavior of the reaction part of

TABLE I. Parameters and variables of the model.

Variables		u CO coverage	
		v O coverage	
		w ratio of the surface in the 1×1 structure	
Parameter			
CO	k_u	Adsorption rate	4.18×10^5 s^{-1} Torr^{-1}
	s_u	Sticking coefficient	1
	u_s	Saturation coverage	1
O_2	k_v	Adsorption rate	7.81×10^5 s^{-1} Torr^{-1}
	s_{v1}	Sticking coefficient on 1×1	0.6
	s_{v2}	Sticking coefficient on 1×2	0.4
	v_s	Saturation coverage	0.8
Rates with $k_i=A_i\exp(-E_i/RT)$			
k_3	Reaction	$A_3=3\times10^6$ s^{-1}	E_r=10 kcal/mol
k_2	CO desorption	$A_2=2\times10^{16}$ s^{-1}	E_d=38 kcal/mol
k_5	Phase transition	A_5=200 s^{-1}	E_p=7 kcal/mol
D	Diffusion coefficient	10^{-10} m^2 s^{-1} (high T)	
J_{io}	Pump rate	360 l s^{-1}	
V	Chamber volume	55 l	

Eqs. (1). Figure 1 displays the bifurcation scenario in the plane of the partial pressures for constant temperature. The stability of the homogeneous oscillation can be tested near the Hopf-bifurcation line by deriving the coefficients of the Ginzburg–Landau equation from the original Eqs. (1).[5,25] The following investigations are restricted to situations with a positive phase-diffusion coefficient, i.e., the homogeneous oscillation is chosen to be stable in the absence of gas-phase coupling.

Simulations of Eqs. (1) and (2) with different strength V_{ML} of the global coupling reveal four different types of patterns: Upon the increase of V_{ML} phase flips, homogeneous oscillations, turbulence, and standing structures are obtained (cf. Fig. 2). The transitions between different patterns depend on the distance of the parameters from the Hopf bifurcation (Fig. 3). The standing structure in Fig. 2 resembles very much the clustering phenomena in networks of coupled oscillators.[26,27] The medium is separated in two large homogeneous domains (clusters), which oscillate with a constant phase difference from each other. A similar phenomenon was recently found in the globally coupled version of the complex Ginzburg–Landau equation.[28] In the following, we will discuss the analogy between these different dynamical systems.

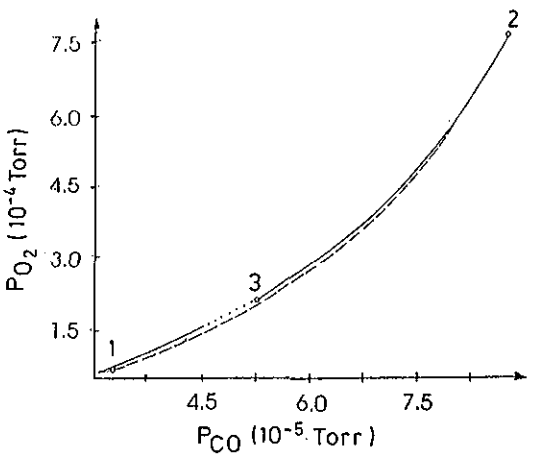

FIG. 1. Simplified bifurcation diagram of Eqs. (1) at T=545 K. The Hopf bifurcation at T=545 K extends from point 1 through point 3 to point 2. The phase diffusion coefficient a has a singularity at point 3 and is negative in the range of the dotted line. The dashed line marks the saddle–node bifurcation.

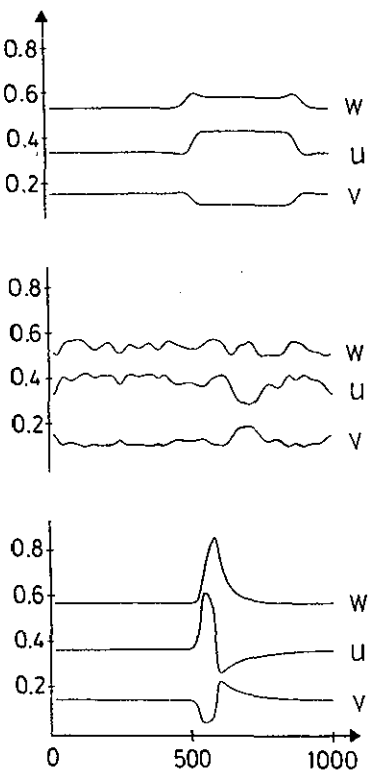

FIG. 2. Typical one-dimensional patterns at p_{O_2} = 1.17 × 10^{-4} Torr, p_{CO_e} = 4.0 × 10^{-5} Torr and T=545 K. *From bottom to top: phase flip* (V_{ML}=0.1 l ML^{-1}), irregular solution (V_{ML}=0.55 l ML^{-1}) and two-cluster solution (V_{ML}=0.65 l ML^{-1}). Here u denotes the CO coverage, v the O coverage and w the ratio of the surface in the 1×1 structure, and z denotes the spatial coordinate. All patterns were obtained with a phase gradient of 2π over the whole integration area as an initial condition.

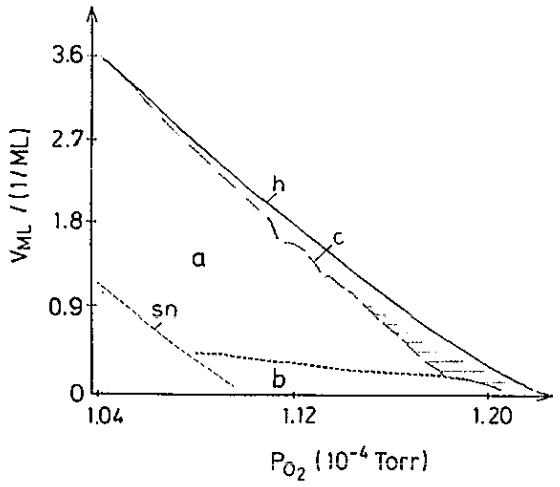

FIG. 3. Phase diagram of one-dimensional patterns at $p_{CO_2} = 4.0 \times 10^{-5}$ Torr and $T=545$ K (sn: saddle–node, h: Hopf bifurcation). (a) Homogeneous oscillations. (b) Phase flips. (c) Two cluster solutions and irregular patterns (hatched region).

Upon consideration of the spatiotemporal dynamics of the cluster pattern in Fig. 2, we find that the oscillators within every subdomain have the same amplitude and phase, but the domains differ from each other with respect to these quantities. In contrast, the period of the oscillations is the same in both clusters. The characteristic features of a cluster state are the size ratio, phase shift, and amplitude ratio of the clusters. A comparison between the system of Eqs. (1) and (2), and a system with pure global coupling (no diffusion) is shown in Fig. 4. The results are almost identical. This indicates that in the cluster states the global coupling is dominant.

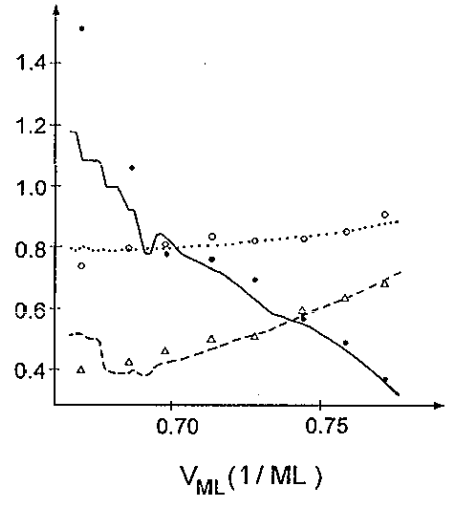

FIG. 4. Characteristic values of clusters in the dependence of V_{ML}. The lines show the values for only globally coupled oscillators, the symbols for locally and globally coupled oscillators: Size ratio—full line, points; amplitude ratio—dashed line, triangles; phase shift—dotted line, circles. The agreement between both systems is quite good for $V_{ML}>0.68$ 1×ML^{-1}.

The conclusion of the preceding section can be backed up by analytical arguments, based on the one-dimensional complex Ginzburg–Landau equation with global coupling, as introduced by Mertens *et al.*:[28]

$$\dot{\eta}=(1-i\omega)\eta-(1+i\beta)|\eta|^2\eta+(1+i\epsilon)\Delta\eta-\mu e^{i\chi}\bar{\eta}. \tag{3}$$

Here $\bar{\eta}$ denotes the spatial average of the complex variable η:

$$\bar{\eta}=\frac{1}{l}\int dx\ \eta(x,t); \tag{4}$$

l is the system length and x is the spatial coordinate. With this equation, cluster states are also obtained as well. But now the stability of the homogeneous oscillation can be calculated analytically (also see Ref. 28). It can be found by calculation of the stability curve, which is given by the dependence of the real part of the eigenvalue λ of the Jacobian, resp., the real part of the Floquet exponent L on the wave number k.[29] The homogeneous oscillation becomes unstable, if the limit of λ with $k\to 0$ is positive (Benjamin–Feir instability). Computation of λ yields the cluster criterion:

$$2\mu\cos\chi-1>0. \tag{5}$$

This criterion being sufficient but not necessary, in case it is not fulfilled, the condition

$$\mu(2+\cos 2\chi+\beta\sin 2\chi)-2(\cos\chi+\beta\sin\chi)<0, \tag{6}$$

will lead to a long-wavelength instability of the homogeneous oscillation.

A similar criterion was found by Hakim and Rappel[27] for a globally coupled network of Ginzburg–Landau-type oscillators. Their model reads as

$$\dot{\eta}_j'=\mu'\eta_j'-(1+i\beta')\eta_j'|^2\eta_j'+\frac{(1+i\epsilon')}{N}\times\sum_{i=1}^{N}(\eta_i'-\eta_j'),\quad j=1,\ldots,N. \tag{7}$$

The cluster criterion for Eq. (7) is given by

$$2\mu'(1+\beta'\epsilon')+1+(\beta')^2<0. \tag{8}$$

If we now consider Eq. (3) without diffusion,

$$\dot{\eta}=\{1+\mu\cos(\chi+\pi)-i[\omega-\mu\sin(\chi+\pi)]\}-(1+i\beta)|\eta|^2\eta+\mu e^{i(\chi+\pi)}(\bar{\eta}-\eta), \tag{9}$$

it can be transformed into Eq. (7) by

$$\eta=[\mu\cos(\chi+\pi)]^{1/2}e^{i[\omega-\mu\sin(\chi+\pi)]\tau}\eta', \tag{10a}$$

$$\tau=\frac{\tau'}{\mu\cos(\chi+\pi)},\quad \mu'=\frac{1+\mu\cos(\chi+\pi)}{\mu\cos(\chi+\pi)}, \tag{10b}$$

and

$$\beta=\beta';\quad \epsilon'=\tan\chi. \tag{10c}$$

Note that $\pi/2<\chi<3\pi/2$ has to be valid now, because the real part of the coefficient of the global coupling term in Eq. (7)

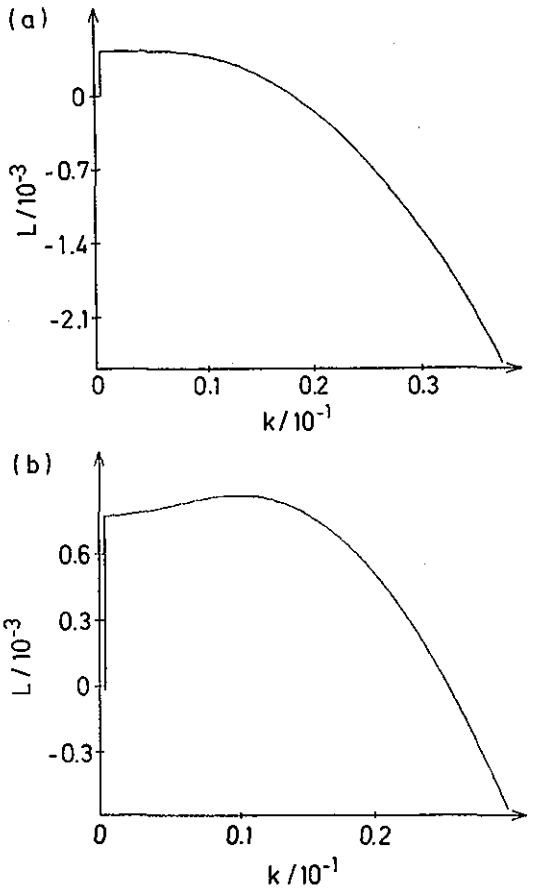

FIG. 5. (a) Stability curve typical for cluster states at $p_{O_2} = 1.193 \times 10^{-4}$ Torr, $p_{CO_2} = 4.0 \times 10^{-5}$ Torr, and $T = 545$ K, $V_{ML} = 0.651 \times ML^{-1}$. Here L denotes the real part of the Floquet exponent. (b) Stability curve with a finite preferred wavelength at $p_{O_2} = 1.68 \times 10^{-4}$ Torr, $p_{CO_2} = 4.734 \times 10^{-5}$ Torr, and $T = 545$ K, $V_{ML} = 0.095\ 1 \times ML^{-1}$.

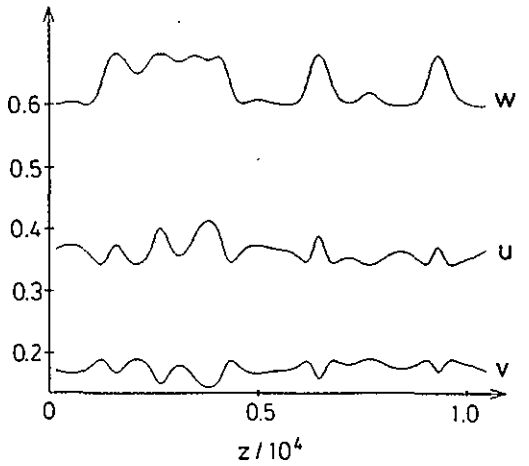

FIG. 6. Modulated cluster state at $p_{O_2} = 1.68 \times 10^{-4}$ Torr, $p_{CO_2} = 4.734 \times 10^{-5}$ Torr and $T = 545$ K and $V_{ML} = 0.095\ 1 \times ML^{-1}$. Here u denotes the CO coverage, v the O coverage and w the ratio of the surface in the 1×1 structure, and z denotes the spatial coordinate.

is assumed to be positive. On the other hand, this implies $\mu' > 1$. Condition (5) in the nomenclature of Eq. (6) reads as $\mu' + 1 < 0$, which condition cannot be met since μ' is positive. Thus, criterion (6) becomes decisive. Indeed, it is found that with the transformation (10) criterion (6) takes on the form of the Hakim and Rappel cluster criterion. This means that clustering sets in at the same parameters, as observed in the numerical simulations with the CO oxidation model (Fig. 1). Because the clustering arises from the global coupling, we can conclude that this regime is completely determined by global interactions, even if local coupling by diffusion is included.

Returning to the reconstruction model of Eqs. (1) and (2), it is obvious that the stability curve $\lambda(k)$ cannot be calculated analytically. Instead, the real part of the largest Floquet exponents $L(k)$ needs to be computed. In the case of clustering, Fig. 5(a) is obtained. There the maximal positive $L = L_{max}$ occurs close to $k = 0$ and $L(k)$ decreases monotonically towards larger wave numbers k. Thus, the selected, fastest growing spatial mode is the one with the wavelength equal to the system size (cf. Fig. 2). Closer to the Hopf bifurcation a modified stability curve $L(k)$ results [Fig. 5(b)]. There L_{max} occurs for $k > 0$, leading to a modulated cluster state (Fig. 6).

At slightly lower p_{O_2}, such modified stability curves already occur for smaller values of V_{ML}. In this regime, the turbulent states are governed by many spatial modes. In the turbulent regime, the spatial modes induce a breakdown of global coupling, which can be illustrated with the change in p_{CO} as an indicator of the coupling strength. Figure 7(a) [7(b)] shows p_{CO} variations in the turbulent regime (a regime with homogeneous oscillations). In both cases, random initial conditions have been used. In Fig. 7(b) one can see how large variations in p_{CO} set in, when all spatial modes are suppressed. In the turbulent case [Fig. 7(a)], the spatial modes survive and the p_{CO} amplitudes remain small.

The standing waves observed in the experiment[11,30] exhibit a typical wavelength (50–100 μm) much smaller than the system size. Therefore the wavelength selection must operate in the experiment, indicating instability of only a finite band of wave numbers and stability (negative real parts of Floquet exponents) of modes close to $k = 0$. Although standing wave patterns have been reported for Eq. (1) in the absence of global coupling,[31] these structures lack an explanation of wavelength selection. In contrast, suitable stability curves and standing waves with a definite wavelength have been obtained in the analysis of the Ginzburg–Landau equation, Eq. (3).[32] Similarly, numerical simulations of the realistic model, Eqs. (1) and (2), close to the transition from cluster states to turbulence (cf. Fig. 2) result in standing waves with wavelengths (~50 μm) comparable to the experimental values. These simulations (Fig. 8) suggest that standing waves are due to a rather delicate balance between local and global coupling, which also appears to agree with experiment, where they were found to be very sensitive to the pump rate (which essentially determines the strength of global coupling).

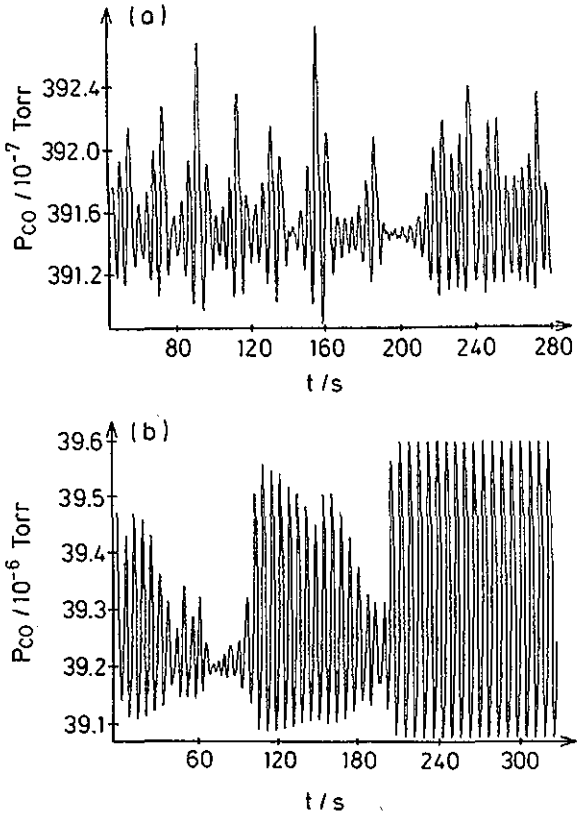

FIG. 7. (a) We see p_{CO} in dependence on time in the turbulent regime at $p_{O_2}=1.16\times10^{-4}$ Torr, $p_{CO_e}=4.10\times10^{-5}$ Torr, and $T=545$ K and $V_{ML}=0.67\,\mathrm{l\,ML^{-1}}$; (b) p_{CO} in dependence on time in the regime with only homogeneous oscillations at $p_{O_2}=1.16\times10^{-4}$ Torr, $p_{CO_e}=4.10\times10^{-5}$ Torr, and $T=545$ K and $V_{ML}=0.65\,\mathrm{l\,ML^{-1}}$.

IV. WAVE INSTABILITIES IN THE EXCITABLE REGIME

A. Backfiring of pulses in one spatial dimension

The CO oxidation model of Eq. (1) can be simplified further by the adiabatic elimination of the variable v (oxygen coverage)[20,21] and rescaling of the variables, space and time, to the final form:[22]

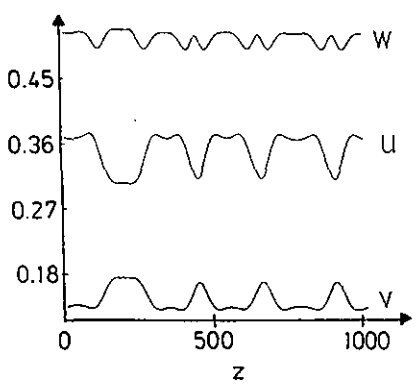

FIG. 8. Standing waves near the transition from turbulent to cluster states ($p_{O_2}=1.17\times10^{-4}$ Torr, $p_{CO_e}=4.0\times10^{-5}$ Torr, $T=545$ K, and $V_{ML}=0.625$ l/ML). For the diffusion constant of Table I, one spatial unit corresponds to 0.2 μm, resulting in a dominant wavelength of about 50 μm.

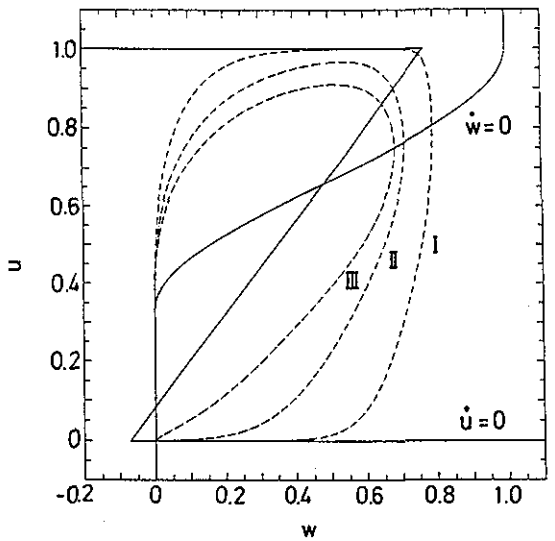

FIG. 9. Null-clines of Eqs. (11) with $a=0.84$ and $b=0.07$. The dashed lines show profiles of solitary pulses for different ϵ (I: $\epsilon=0.04$, II: $\epsilon=0.07$, III: $\epsilon=0.10$), indicating a shrinking refractory tail ($u=0$, $v>0$) for increasing ϵ.

$$\frac{\partial u}{\partial t}=-\frac{1}{\epsilon}u(u-1)\left(u-\frac{w+b}{a}\right)+\Delta u, \tag{11a}$$

$$\frac{\partial w}{\partial t}=g(u)-w. \tag{11b}$$

The function $g(u)$ is obtained from the original form $f(u)$ by the rescaling process. For excitable conditions, we used the form

$$g(u)=\begin{cases}0, & u<\frac{1}{3}\\ 1-6.75u(u-1)^2, & \frac{1}{3}\leqslant u\leqslant 1,\\ 1, & u>1.\end{cases} \tag{11c}$$

Note that p_{CO}, P_{O_2}, and T are cast into the new parameter set a, b, and ϵ. Excitable conditions in Eqs. (11) can be realized by a choice of $a<1$ and $b>0$ and smaller. For more details of the mapping between Eqs. (1) and Eqs. (11), the reader is referred to Ref. 22. Equations (11) are similar to the model proposed by Barkley, and were integrated by the procedures described in his paper.[33] The computational efficiency of the form (11) enabled us to carry out systematic investigations of the parameter space (a,b,ϵ).

From Eqs. (11) it is clear that the CO oxidation belongs to the class of activator(u)–inhibitor(w) models, which have been frequently used in the investigation of excitable media. The equations might be described as a modified FitzHugh–Nagumo model (FHN)[34] with delayed inhibitor production,[35] which is given by the specific form of $g(u)$. This delay of the inhibitor production, which starts only above a threshold value of $\frac{1}{3}$ of u, leads to two additional unstable fixed points for excitable conditions, as shown in the null-cline portrait of Fig. 9. The standard FHN model as well as the Oregonator model[34] contain a proportionality between inhibitor production and activator concentration $[g(u)=u]$. The delay in the

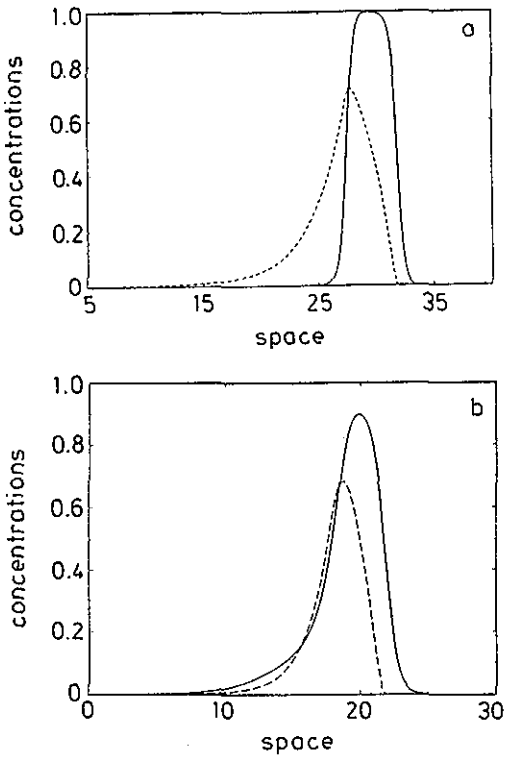

FIG. 10. Spatial pulse profiles of activator (u, solid line) and inhibitor concentration (w, dashed line) for $a=0.84$ and $b=0.07$. ϵ—values are 0.04 *(top)* and 0.105 *(bottom)*. Note that in the lower graph the refractory zone has almost vanished ($\epsilon_c=0.107$ for backfiring).

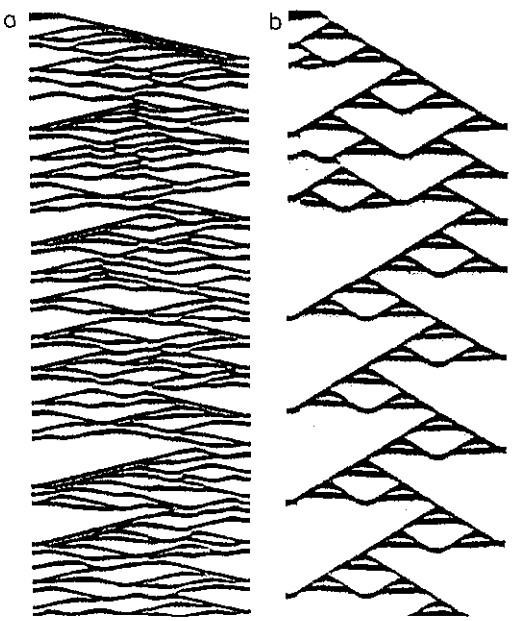

FIG. 11. Two examples for space-time plots arising from the backfiring instability at $a=0.84$ and $\epsilon=0.11$ in Eqs. (11). (a) $b=0.09$, turbulent state and (b) $b=0.18$, periodic state, after a short transient. The vertical axis is time, the horizontal one space.

inhibitor production facilitates pulse propagation at unusually big values of ϵ in the one-dimensional version of Eqs. (11). Inspection of the pulse profiles for constant a and b shows that the refractory zone of the pulses became smaller with increasing ϵ and vanished at some critical value $\epsilon_c=0.107$ (Fig. 10). For $\epsilon>\epsilon_c$, reexcitation behind the pulse appeared and created new pulses. This "backfiring" process led to complicated space-time plots, which are either turbulent or periodic (Fig. 11). The turbulent behavior is the dominating outcome of the instability, periodic states were observed only close to the onset of backfiring and in not too long systems. Since colliding pulses annihilate upon collision, backfiring could also manifest itself in the creation of a transient irregular state, which fell back into the stable rest state of the medium after some time.

For $a=0.84$, the backfire transition is observed between $b=0$ and $b=0.18$ (see the phase diagram below). Upon the further increase of ϵ far beyond the backfire threshold, a stable limit cycle is created around the upper unstable fixed point (compare Fig. 9) through a saddle–loop bifurcation. Finally, this limit cycle vanishes by a Hopf bifurcation, resulting in a bistable system.

Inside the turbulent regime, the following change in dynamics was observed: With increasing ϵ, the backfiring became more frequent. This led to a higher density of pulses in the system and to more frequent annihilation events. At still higher ϵ, the pulse character disappears and global oscillations of turbulent nature take over. A calculation of the Lyapunov dimension revealed that the medium can be classified as spatiotemporally chaotic,[36] since this quantity was shown to be extensive, i.e., its value was proportional to the system length.[37]

B. Spiral breakup in two spatial dimensions

The pulse instability should have its counterpart in the two-dimensional version of Eqs. (11). In two dimensions, spiral waves are the most frequent patterns in excitable media.[6,38,39] Their behavior was investigated in a couple of models.[34,40,41] Remarkably, in most systematic studies, spiral waves turned out to be very robust structures. The only instability was the change from a steady rotation to a meandering motion of the spiral tip,[42,43] which could be identified as a Hopf bifurcation.[44] For sufficiently big values of ϵ, the spiral wave solutions disappeared. At the boundary the spiral period and the core size diverged. In contrast to this picture, the model of Eqs. (11) showed a breakup of spirals at sufficiently big values of ϵ, which led to a turbulent pattern (Fig. 12).

This spiral instability can be rationalized as follows: The dispersion relation in excitable media exhibits a minimum temporal period $\tau_{\min}$, below which no periodic wave train solutions exist. Both quantities follow typical scaling laws:

$$\tau_{\min}\propto\epsilon^{\alpha} \quad \text{and} \quad \tau_0\propto\epsilon^{\gamma}. \tag{12}$$

When ϵ is increased, this minimum period allowed by the dispersion relation grows faster than the rotation period τ_0 of the spiral, i.e., $\alpha>\gamma$. The exponent γ was derived analytically in the low-ϵ limit to be $\frac{1}{3}$.[11] Numerical simulations[6] yielded approximately $\frac{1}{2}$ for α and $\frac{1}{3}$ for γ. Both results were obtained by use of the FitzHugh–Nagumo model. With the

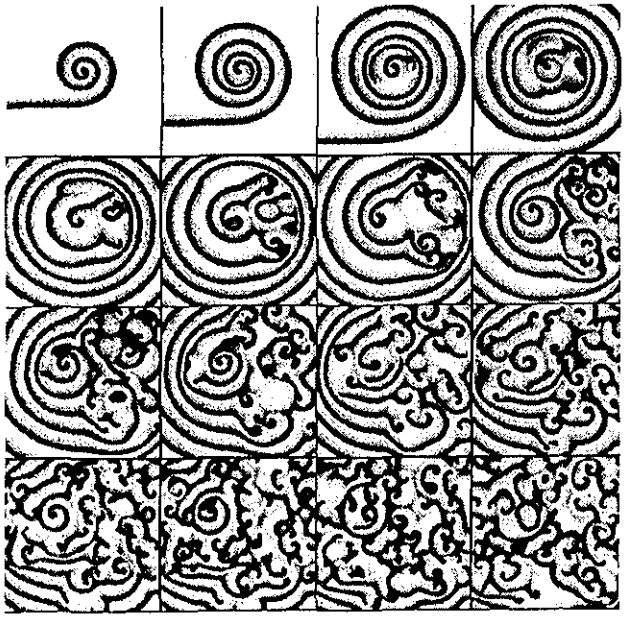

FIG. 12. Development of turbulence at $a=0.84$, $b=0.07$, and $\epsilon=0.08$. The area of one picture is 100×100 (grid points used: 256×256). The time difference between pictures is 6.41. The inhibitor concentration is shown in grey values.

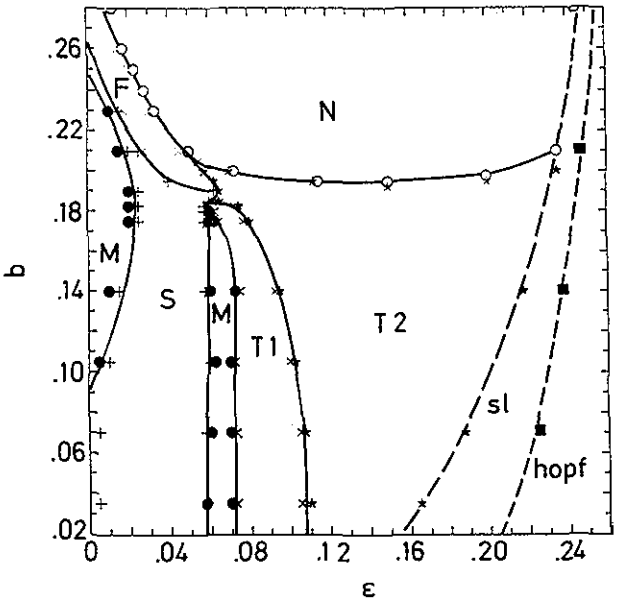

FIG. 14. Phase diagram revealing regions of different waveforms ($a=0.84$): spirals with rigid rotation (S); meandering spirals (M); turbulence 1 (T1, spiral breakup); turbulence 2 (T2, backfiring); no waves (N). Dotted lines show bifurcations in the reaction part of Eqs. (11). The saddle–loop bifurcation (sl) creates a stable limit cycle around the unstable fixed point. This limit cycle is then destroyed by a Hopf bifurcation (Hopf), which changes the unstable node to a stable one.

present model, these values are $\alpha=0.7$ and $\gamma=0.4$ (taken from Fig. 13 at $\epsilon<0.06$). Spirals become unstable if the two values τ_0 and τ_{min} merge, because the periodic sequence of spiral arms has to fulfill the dispersion relation, i.e., $\tau_0>\tau_{min}$. It should be noted that τ_{min} was calculated in one dimension and can be corrected by inclusion of the curvature effect.[45]

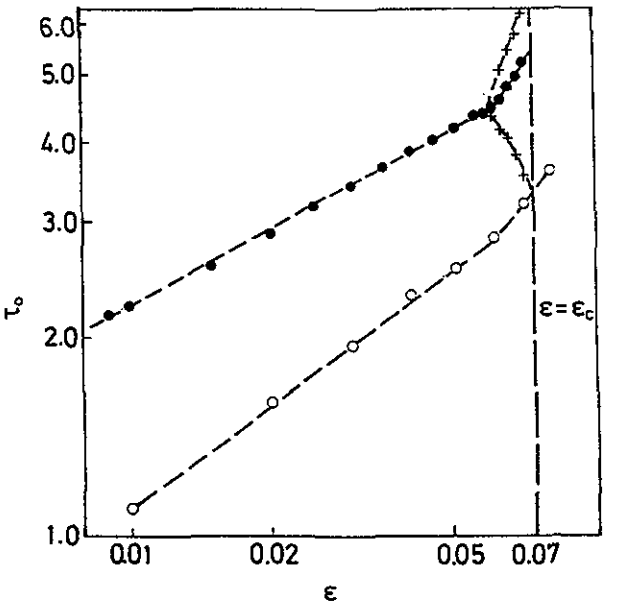

FIG. 13. Spiral rotation period τ_0 at fixed $a=0.84$, $b=0.07$ for different values of ϵ. After the onset of meandering ($\epsilon=0.06$), the mean period is drawn (full circles), while crosses show the maximum and minimum period near the spiral center. At $\epsilon=\epsilon_c$, the latter falls below the minimum period allowed by the dispersion relation (open circles) so that the spiral breaks.

Here we neglect this additional aspect. After the onset of meandering, the resulting motion of the spiral core gets faster with growing ϵ, and consequently a large variation of the period due to the Doppler effect appears in the inner spiral arms (i.e., the meandering tip is regarded as a moving source of periodic waves;[13] Fig. 13). Finally, the smallest period caused by the Doppler effect fell below the minimum period of wave trains in the one-dimensional system (as given by the dispersion relation computed according to Ref. 6). Thus, in the propagation direction of the tip, the waves are pressed too close together.

Since the scaling laws with the given exponents are claimed to be universal,[39,46,47] similar behavior should be expected in other models. The trouble is that these laws are usually valid only for very small ϵ and that τ_0 grows much faster for larger ϵ, and finally diverges at the spiral boundary, thus preventing the merging of τ_0 and τ_{min} seen in the present model (Fig. 13). In other words, the delayed inhibitor production helps to conserve both the scaling laws in Eq. (12) and the existence of spiral waves toward sufficiently big values of ϵ, thus enabling the breakup phenomena.

The breakup in Eqs. (11) was observed for b values smaller than $b=0.18$ at $a=0.84$. The phenomenon was always preceded by a meandering instability in the excitable case, and the instability occurred at comparable values of ϵ (near $\epsilon=0.07$). At $b>0.18$, the usual transition with diverging periods and a small regime of shrinking flat waves was found (Fig. 14). We should mention that meandering is not a necessary prerequisite of spiral breakup, it only shifts the stability threshold to smaller ϵ. A direct transition from stable

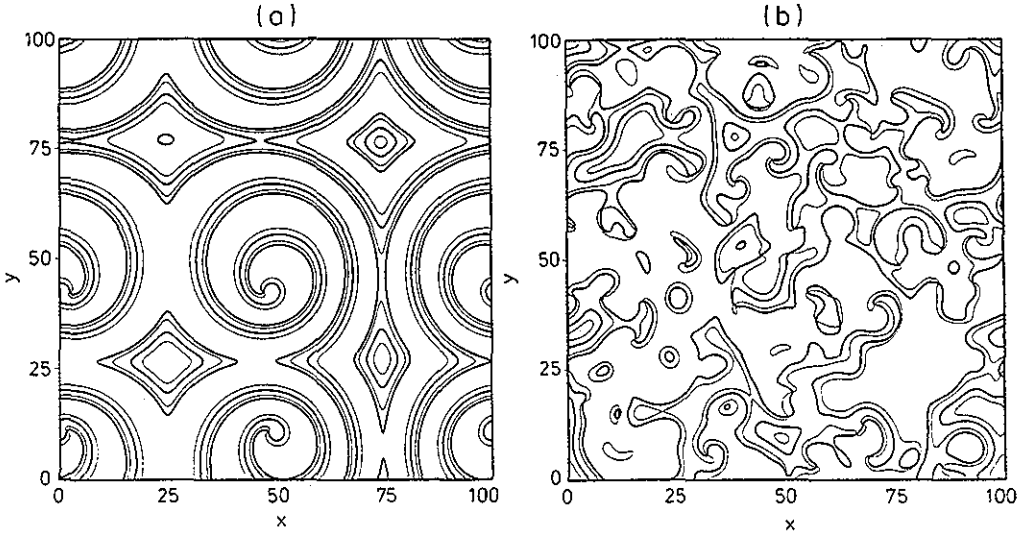

FIG. 15. Snapshots of isoconcentration contours $u=0.66$ (thin lines) and $w=0.484$ (thick lines) for $a=0.84$ and $b=0.07$. (a) Four stable spirals ($\epsilon=0.07$). (b) Turbulent state with about 80 topological defects ($\epsilon=0.10$).

spirals to turbulence via breakup was seen in Eqs. (11) for oscillatory conditions at negative b for $a=0.84$ and ϵ near 0.08.[45]

There exist several other examples of spiral breakup in excitable reaction-diffusion systems.[48–50] One of these authors also used scaling arguments[50] to explain the breakup. In this case, besides meandering another instability, which was first discovered in the one-dimensional system,[51] occurred and was made responsible for the spiral instability.

Another important topic is the characterization of the turbulence originating from the spiral breakup. A suitable tool is provided by the analysis of the number of topological defects, which are given by the intersection of the u and v contours corresponding to the upper unstable fixed point in Fig. 9. Two examples of such a contour plot in the cases of stable spirals and chemical turbulence are displayed in Fig. 15. The topological defects below ϵ_c simply represent the tip of the stable spirals. Their number is constant. In contrast, the breakup of spirals and their subsequent self-replication led to an increase in the number $n(t)$ of topological defects, until a certain defect density is reached, and the creation of new defects is balanced with mutual annihilation. The number $n(t)$ then fluctuated around a constant mean value, as is demonstrated in Fig. 16. Close to the breakup transition, very long transients in $n(t)$ were found, and the variance of the defect number $n(t)$ was considerably smaller than the mean value of $n(t)$ itself (sub-Poissonian distribution). Far away from ϵ_c, the variance increased and approached the mean value (similar to what was obtained for defect-mediated turbulence in the complex Ginzburg–Landau equation[52,53]). The long transients resulted from a slower propagation of the turbulence into the medium. The increase in the variance is caused by a higher mobility of defects.

The spiral instability as well as the pulse instability described in this chapter are examples of an excited turbulence, which appears only due to the application of a specific threshold perturbation (creation of a pulse or a spiral seed) to an otherwise homogeneous and stable rest state of the medium. To conclude, we should point out that the results presented in Sec. II were obtained with small values of ϵ, where wave trains and spirals were stable in the absence of global coupling. Thus, the turbulence reported there is clearly due to the influence of changes in the gas phase.

V. CONCLUSION

We presented simulation results with the reconstruction model of the CO oxidation on Pt(110). The introduction of gas-phase coupling into the model equations under oscillatory conditions led to the formation of standing structures and turbulent patterns, depending on the coupling strength.

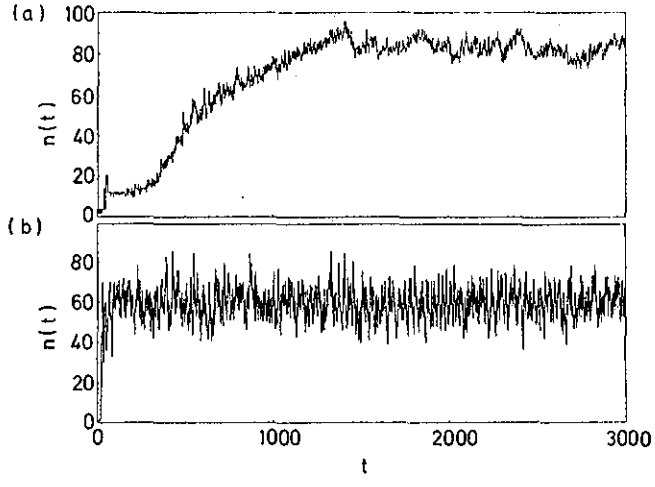

FIG. 16. The number of topological defects $n(t)$ versus time for $a=0.84$ and $b=0.07$; (a) near the onset of turbulence ($\epsilon=0.072$), (b) farther away from it ($\epsilon=0.10$).

The experimentally observed wavelength selection was found only at the boundary between these two types of behavior. This indicated a critical balance between local and global coupling. The standing waves lost their characteristic length scale, if global coupling dominated.

In the excitable regime of the reaction, variation of the rate constants resulted in the discovery of characteristic wave instabilities of pulses (backfiring) and spirals (breakup).

Experimentally, it is difficult to distinguish whether the underlying dynamics of a turbulent state is oscillatory or excitable. Also, the initial conditions are hard to control so that well-defined transients could not be observed. It is therefore not yet clear by which of the described scenarios turbulence forms in the experiments or whether both can occur. The suggested characterization tools for chemical turbulence via defect statistics may help to clarify this point in future studies.

ACKNOWLEDGMENT

Financial support by Deutsche Forschungsgemeinschaft is greatly appreciated.

[1] M. C. Cross and P. C. Hohenberg, Rev. Mod. Phys. **65**, 851 (1993).
[2] G. Ahlers, Physica D **51**, 421 (1991).
[3] *Oscillations and Traveling Waves in Chemical Systems*, edited by R. J. Field and M. Burger (Wiley, New York, 1985).
[4] J. Ross, S. C. Müller, and C. Vidal, Science **240**, 460 (1988).
[5] Y. Kuramoto, *Chemical Oscillations, Waves, and Turbulence* (Springer-Verlag, Berlin, 1984).
[6] J. J. Tyson and J. P. Keener, Physica D **32**, 327 (1988).
[7] W. Jahnke and A. T. Winfree, Int. J. Bifurcation Chaos **1**, 445 (1991).
[8] G. Ertl, Adv. Catal. **40**, 213 (1990).
[9] K. Krischer, M. Eiswirth, and G. Ertl, J. Chem. Phys. **96**, 9161 (1992).
[10] M. Eiswirth, P. Möller, K. Wetzl, R. Imbihl, and G. Ertl, J. Chem. Phys. **90**, 510 (1989).
[11] S. Jakubith, H. H. Rotermund, W. Engel, A. von Oertzen, and G. Ertl, Phys. Rev. Lett. **65**, 3013 (1990).
[12] G. Ertl, Science **254**, 1750 (1991).
[13] P. Coullet, L. Gil, and J. Vega, Phys. Rev. Lett. **62**, 1619 (1989).
[14] G. Huber, P. Alstrom, and T. Bohr, Phys. Rev. Lett. **69**, 2380 (1992).
[15] T. Engel and G. Ertl, Adv. Catal. **28**, 1 (1979).
[16] R. P. H. Gasser, *An Introduction to Chemisorption and Catalysis by Metals* (Clarendon, Oxford, 1985).
[17] R. Gomer, Rep. Prog. Phys. **53**, 917 (1990).
[18] A. von Oertzen, Thesis, Freie Universität Berlin, 1992.
[19] M. Bär, M. Eiswirth, H. H. Rotermund, and G. Ertl, Phys. Rev. Lett. **69**, 945 (1992).
[20] M. Bär, Ch. Zülicke, M. Eiswirth, and G. Ertl, J. Chem. Phys. **96**, 8595 (1992).
[21] M. Falcke, M. Bär, H. Engel, and M. Eiswirth, J. Chem. Phys. **97**, 4555 (1992).
[22] M. Bär, N. Gottschalk, M. Eiswirth, and G. Ertl, J. Chem. Phys. **100**, 1202 (1994).
[23] S. Nettesheim, A. von Oertzen, H. H. Rotermund, and G. Ertl, J. Chem. Phys. **98**, 9977 (1993).
[24] M. Falcke and H. Engel, submitted to J. Chem. Phys.
[25] M. Falcke and H. Engel, in *Spatio-Temporal Organization in Nonequilibrium Systems*, edited by S. C. Müller and T. Plesser (Projekt-Verlag, Dortmund, 1992),
[26] D. Golomb, D. Hansel, B. Shraiman, and H. Sompolinsky, Phys. Rev. A **45**, 3516 (1992).
[27] V. Hakim and W. J. Rappel, Phys. Rev. A **46**, R7437 (1992).
[28] F. Mertens, R. Imbihl, and A. Mikhailov, J. Chem. Phys. **99**, 8668 (1993).
[29] M. Falcke, M. Neufeld, and H. Engel (unpublished).
[30] K. Krischer, R. Rico-Martinez, I. G. Kevrekidis, H. H. Rotermund, G. Ertl, and J. L. Hudson, AIChE J. **39**, 89 (1993).
[31] H. Levine and X. Zou, Phys. Rev. E **48**, 50 (1993).
[32] F. Mertens, R. Imbihl, and A. S. Mikhailov, J. Chem. Phys. (in press).
[33] D. Barkley, Physica D **49**, 61 (1991).
[34] A. T. Winfree, Chaos **1**, 303 (1991).
[35] M. Bär and M. Eiswirth, Phys. Rev. E **48**, R1635 (1993).
[36] M. C. Cross and P. C. Hohenberg, Science **263**, 1569 (1994).
[37] M. Hildebrand, M. Bär, Th.-M. Kruel, and M. Eiswirth (unpublished).
[38] A. S. Mikhailov, *Foundations of Synergetics* (Springer-Verlag, Berlin, 1990).
[39] E. Meron, Phys. Rep. **218**, 1 (1992).
[40] A. M. Pertsov, E. A. Ermakova, and A. V. Panfilov, Physica D **14**, 117 (1984).
[41] D. Barkley, M. Kness, and L. S. Tuckerman, Phys. Rev. A **42**, 2489 (1990).
[42] A. S. Mikhailov, V. S. Zykov, and V. A. Davydov, Physica D **70**, 1 (1993).
[43] D. Barkley, Phys. Rev. Lett. **72**, 164 (1994).
[44] D. Barkley, Phys. Rev. Lett. **68**, 2090 (1992).
[45] M. Bär, M. Hildebrand, and M. Eiswirth (unpublished).
[46] P. C. Fife, CBMS-NSF Conf. Ser. Appl. Math. **53**, 1 (1989).
[47] A. Karma, Phys. Rev. Lett. **68**, 397 (1992).
[48] M. Courtemanche and A. T. Winfree, Int. J. Bifurcation Chaos **1**, 431 (1991).
[49] A. Panfilov and P. Hogeweg, Phys. Lett. A **176**, 295 (1993).
[50] A. Karma, Phys. Rev. Lett. **71**, 1103 (1993).
[51] M. Courtemanche, L. Glass, and J. P. Keener, Phys. Rev. Lett. **70**, 2182 (1993).
[52] L. Gil, J. Lega, and J. L. Meunier, Phys. Rev. A **41**, 1138 (1990).
[53] I. Aranson, L. Kramer, and A. Weber, Phys. Rev. Lett. **72**, 2316 (1994).